Reaction Mechanism Based on X-ray Crystal Structure Analysis during the Solid-State Polymerization of Muconic Esters

Daisuke Furukawa and Akikazu Matsumoto*

Department of Applied Chemistry, Graduate School of Engineering, Osaka City University, Sugimoto, Sumiyoshi-ku, Osaka 558-8585, Japan

Received April 4, 2007; Revised Manuscript Received June 26, 2007

ABSTRACT: We have investigated a change in the crystal structures of di(4-alkoxybenzyl) (*E*,*E*)- and (*Z*,*Z*)-muconates during the solid-state polymerization by X-ray crystal structure analyses and have discussed a reaction mechanism for the polymerization. The solid-state polymerization is divided into a homogeneous polymerization which proceeds in the solid solution of the remaining monomer and the resulting polymer and a heterogeneous polymerization in which a crystal phase separation occurs between the monomer and polymer crystal domains during the reaction. According to the former model, the monomer crystal phase continuously changes into the polymer crystal phase without any phase separation when the slightest movement of atoms induces less strain in the crystals. The molecular dynamics of the muconates in the solid state were monitored by *in situ* single and powder X-ray diffraction experiments. In fact, we succeeded in the direct observation of the expanding crystal lattices and cell volume at the initial stage of polymerization, followed by subsequent shrinking in the process of the homogeneous reaction. On the other hand, a phase separation was observed during the reaction according to the heterogeneous polymerization model, in which a considerable movement of atoms is required. The monomer stacking structure determines the reaction path during the solid-state polymerization.

Introduction

Crystalline-lattice-controlled organic reactions provide a product with a high selectivity in the solid state.[1−11] In particular, a topochemical reaction is defined as a reaction that occurs with the minimum movement of atoms in the solid state and where the symmetry of the product crystal is the same as that of the starting crystal.[12] As a result, a topochemical reaction is useful for the design of solid materials with extremely controlled molecular and crystalline structures. Crystal engineering was already established in the middle of the 1970s based on the results for [2 + 2] photodimerization,[13−15] and thereafter, a large number of studies have been reported on solid-state reactions including the topochemical polymerization of unsaturated compounds[16−26] as well as various kinds of solid-state polymerization.[27−31]

During the recent decade, we have demonstrated the topochemical polymerization of 1,3-diene monomers to give polymer crystals. We revealed that the polymerization of muconic derivatives occurs not only under UV irradiation but also under X- and γ-ray radiation.[32−39] The reactivity of topochemical polymerization via a chain reaction mechanism is determined by a common principle; the polymerization readily occurs when diene monomer molecules are arranged in a columnar structure in the crystals with a stacking distance of 5 Å.[40] In addition, it was already reported that di(4-methoxybenzyl) muconates favor an alternate stacking structure supported by weak CH/π and CH/O interactions and provide a stereoregular polymer with a disyndiotactic repeating structure.[41,42]

The di(4-alkoxybenzyl) esters of (*E*,*E*)- and (*Z*,*Z*)-muconic acids are different geometric structures, but the obtained polymers have completely identical chemical structures with the same tacticity[43] (Scheme 1). Recently, we have revealed a change in the structure of the crystals of some muconic esters accompanied by the shrinking and expanding of the lattice lengths, on the basis of the X-ray single-crystal structure analysis of the monomers and polymers as well as a change in the transient structure monitored by powder X-ray diffraction during the continuous X-ray radiation.[44] A lattice length in the direction along the fiber axis decreases during the polymerization, where monomers are arranged in a columnar assembly with a stacking distance greater than the fiber period of the resulting polymer. The polymerization rate is closely related to the molecular stacking distance in the monomer crystals because the polymer chain skeletons have the same conformational structure in the crystals.[44]

Scheme 1

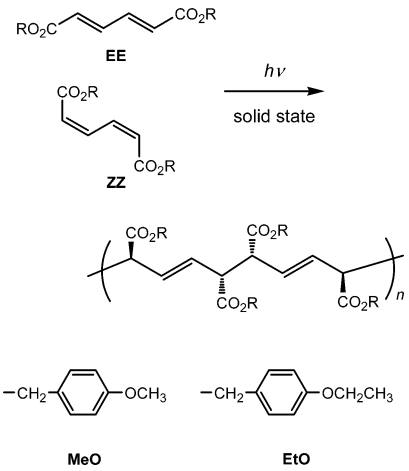

On the other hand, intensive studies have been carried out for the reaction mechanism of the solid-state polymerization of diacetylene compounds since the 1970s.[16−18,45,46] Wegner and co-workers[16,47,48] first reported a mechanistic model as well as

* Corresponding author. E-mail: matsumoto@a-chem.eng.osaka-cu.ac.jp.

10.1021/ma070802f CCC: $37.00 © 2007 American Chemical Society
Published on Web 07/31/2007

the experimental evidence of single-crystal-to-single-crystal transformation during the polymerization of diacetylene in the solid state. In their model, a monomer single-crystal transforms into the corresponding polymer single crystal by the least movement of the atoms, and the center of the molecular mass of the reacting molecules remains in the same position in the crystal lattice. Homogeneous and heterogeneous reactions as well as phase transition from monomer to polymer crystals have also been discussed for the solid-state polymerization of diacetylene and diolefin derivatives.[49−52] Thereafter, more progressed reaction models were proposed for the solid-state polymerization of diacetylenes.[53−60] The phase transition of the monomer crystals into the polymer crystals during the polymerization is important when the reaction mechanism of solid-state polymerization is discussed. In fact, a drastic and discontinuous change in the crystal structure is often observed during the solid-state polymerization of diacetylene and 1,3-diene derivatives.

In the present study, we have investigated the molecular dynamics during the solid-state polymerization of di(4-methoxybenzyl) (*E*,*E*)-muconate (**EE-MeO**), di(4-methoxybenzyl) (*Z*,*Z*)-muconate (**ZZ-MeO**), di(4-ethoxybenzyl) (*E*,*E*)-muconate (**EE-EtO**), and di(4-ethoxybenzyl) (*Z*,*Z*)-muconate (**ZZ-MeO**), as shown in Scheme 1. A structural change during the polymerization was monitored by *in situ* single and powder X-ray diffraction experiments. We also found some polymerizations accompanied by a crystal phase separation, while the other polymerizations homogeneously occur in the solid state. We discuss a reaction mechanism for the solid-state polymerization that proceeds via a chain reaction mechanism with or without crystal phase separation occurring during the reaction of the muconates.

Experimental Section

Materials and General Procedures. Muconic acid was purchased from Across Organics or Aldrich Co., Ltd., and used without further purification. The benzyl esters were prepared by the reaction with 4-methoxy- and 4-ethoxybenzyl bromides according to the procedure described in the previous paper.[61] The NMR and IR spectra were recorded using JEOL JMN A-400 and JASCO FT/IR-430 spectrometers, respectively, at room temperature. γ-Radiation was carried out with ^{60}Co at room temperature at Osaka Prefecture University. The irradiation dose was 200 kGy. Monomer single crystals were cut to an appropriate size and γ-radiated for the fabrication of polymer single crystals.

Crystal Structure Determination. The crystals were obtained by slow evaporation from a chloroform solution. Single-crystal X-ray diffraction data were collected using a Rigaku RAXIS RAPID imaging plate diffractometer with Mo Kα radiation (λ = 0.71073 Å) monochromated by graphite. The crystal structures were solved by a direct method using SIR92 and refined by the full-matrix least-squares method on F^2 with anisotropic displacement parameters for non-hydrogen atoms using SHELXL-97. Single-crystal structure analysis was carried out at −150 °C for **EE-MeO**, **ZZ-MeO**, poly(**EE-MeO**), and poly(**ZZ-MeO**). In our previous paper,[41] the crystal structures were determined at −70 °C for **EE-MeO** and **ZZ-MeO** and at room temperature for poly(**EE-MeO**) and poly(**ZZ-MeO**), and similar packing structures were obtained. However, the lattice parameters obtained in the present study are different from the previous parameters beyond the expectation of temperature effects, due to polymorphs with a similar packing structure. Because **EE-EtO** as well as the corresponding polymer gave a single crystal with a lower quality, we determined the crystal structures under limited conditions. In order to monitor a change in the single-crystal structure of **EE-MeO** during the polymerization, the single crystal of **EE-MeO** was irradiated with an X-ray beam at specified time intervals at room temperature, and each crystal structure was determined at −150 °C to avoid the effect of polymerization during the structure determination. Each conversion was determined on the basis of site occupancy factors of monomer and polymer structures.

The powder X-ray diffraction profile was recorded using a Rigaku RINT-2100 diffractometer with monochromated Cu Kα radiation (λ = 1.54184 Å, 40 kV, 40 mA, scan speed 1.0 °/min), equipped with a high-resolution parallel-beam optics system consisting of a parallel slip analyzer PSA100U and a graded multiplayer 2960C1. The polymerization of powdery crystals occurred under X-ray beam radiation conditions during X-ray diffraction measurement at room temperature. The samples were crushed with a mortar and pestle to below 100 μm in their crystal grain size. The scan range for the diffraction measurement was 3−40° for the **EE-** and **ZZ-MeO** crystals and 10−30° for the **EE-** and **ZZ-EtO** crystals. The observed diffraction lines were indexed by comparison with the simulated diffraction profiles based on the single-crystal structures. The conversion was determined from a change in the absorption intensity of the C=C stretching around 1600 cm^{-1} using the same sample by diffuse reflectance IR spectroscopy.[39] Using eq 1 for a monoclinic system, each lattice length was estimated from the 2θ values of the indexed peaks with the assumption that the β angle is constant at 100°.

$$\frac{1}{d_{hkl}^2} = \frac{1}{\sin^2\beta}\left(\frac{h^2}{a^2} + \frac{k^2\sin^2\beta}{b^2} + \frac{l^2}{c^2} - \frac{2hl\cos\beta}{ac}\right) \quad (1)$$

Results and Discussion

The single-crystal structures of **EE-MeO** and **ZZ-MeO** were determined at −150 °C to avoid the effect of the polymerization. The polymer single crystals were obtained by γ-radiation polymerization, and their crystal structures were determined under the same conditions. The crystal structure and crystallographic data are summarized in Figure 1, parts a−c and Table 1. The change in the lattice parameters before and after the polymerization is small, because the polymerization occurs via a topochemical reaction mechanism. The magnitude of the change in the lattice length, angle, and cell volume was 0.2−3.0% during the polymerization of **EE-MeO**. These values are much smaller than those of **ZZ-MeO** (2.7−6.8%). Interestingly, poly(**EE-MeO**) and poly(**ZZ-MeO**) crystals have completely identical structures regarding not only the stereochemical structure (tacticity) but also the crystal structure (molecular conformation). In other words, both polymer crystals have the same crystallographic parameters. This indicates that a greater movement of atoms is required in the crystals of **ZZ-MeO** than in **EE-MeO** during the polymerization.

Similarly, the crystal structures of **ZZ-EtO** and **EE-EtO** as the ethoxy derivatives were also investigated. The single-crystal structure of poly(**EE-EtO**) could not be determined in the present study because of the difficulty of the preparation of high-quality single crystals of the **EE-EtO** monomer. The crystal structure is shown in Figure 1d−f. As shown in the crystallographic parameters in Table 1, we obtained the crystal structure under the limited temperature conditions and with limited accuracy of the data. Nevertheless, we can conclude that the ethoxy-substituted benzyl muconates have a molecular packing structure similar to those for the methoxy derivatives and that the polymerization of **ZZ-EtO** also occurs via a topochemical polymerization mechanism.

A change in the molecular structure is detected by *in situ* X-ray structure analysis when the crystals maintain its high quality during the solid-state reactions. In the present study, we carried out powder and single-crystal structure analyses to monitor the reaction, in which the polymerization rate can be controlled by temperature and the intensity of the used X-ray

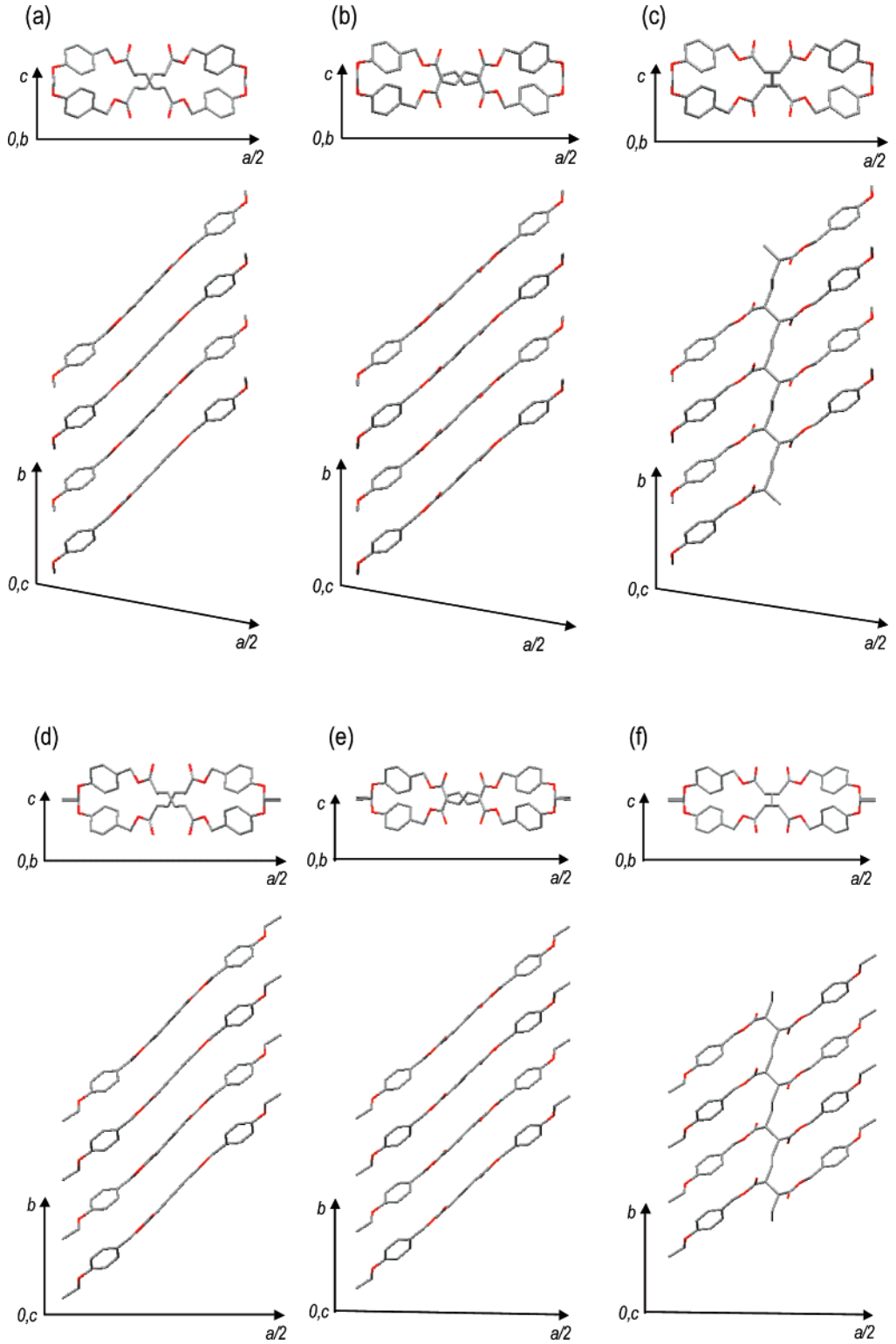

Figure 1. Crystal structures of (a) **EE-MeO**, (b) **ZZ-MeO**, (c) poly(**ZZ-MeO**), (d) **EE-EtO**, (e) **ZZ-EtO**, and (f) poly(**ZZ-EtO**). Poly(**EE-MeO**) has the same structure as part c.

beam. First, we examined the change in the crystal lattice for **EE-MeO** and **ZZ-MeO** by continuous X-ray radiation at room temperature. Figure 2 shows the change in powder X-ray diffraction profiles observed during the polymerization of **EE-MeO** and **ZZ-MeO**. At the same time, the conversion of monomer to polymer was determined from a change in the absorption intensity of the C═C stretching around 1600 cm^{-1} by diffuse reflectance IR spectroscopy. The conversion increased with the scan numbers of the radiation for the powder X-ray measurement. Table 2 summarizes a change in the position, intensity, and half-line width of the characteristic diffraction line (d_{600}), as well as the conversion at each scan number.

For the powder X-ray diffractions of the **EE-MeO** crystals in Figure 2a, all diffraction lines continuously shifted from a position for the monomer to that for the polymer without broadening of the line. The half-line width values for **EE-MeO** shown in Table 2 are constant in the range of 0.21−0.28. On the other hand, **ZZ-MeO** provided quite different results. The diffraction lines showed a discontinuous change under the same radiation conditions. The profiles of the diffraction from the

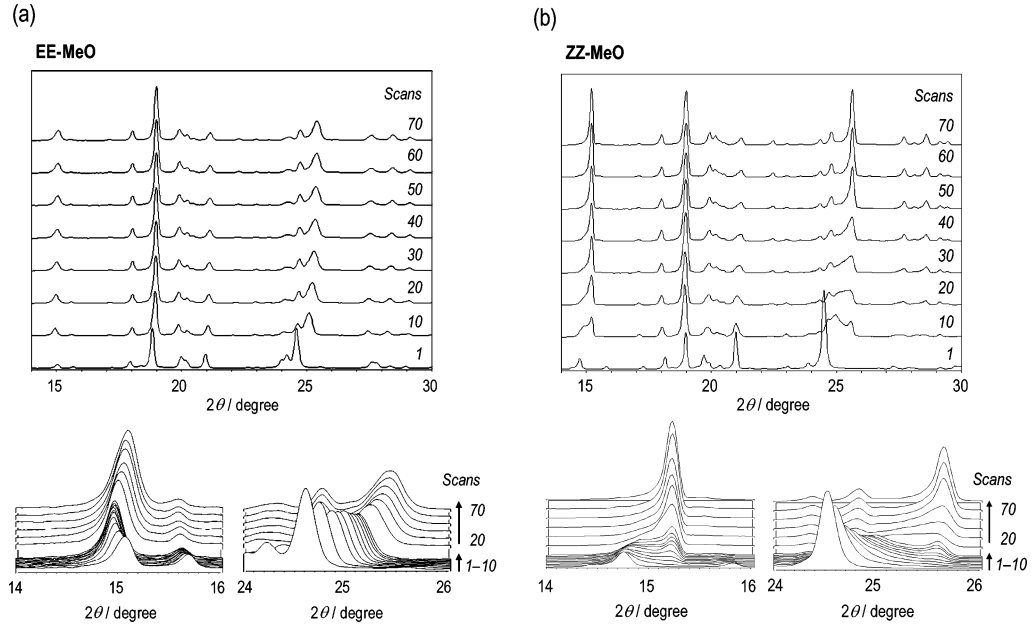

Figure 2. Change in powder X-ray diffraction profiles during the polymerization of (a) **EE-MeO** and (b) **ZZ-MeO** at room temperature. The expanded diffraction lines around 15 and 25° were assigned to d_{600} and d_{80-2}, respectively.

Table 1. Crystallographic Data of Monomer and Polymers

	EE-MeO	**ZZ-MeO**	poly(**EE-MeO**)	poly(**ZZ-MeO**)
cryst syst	monoclinic	monoclinic	monoclinic	monoclinic
space group	*C*2/c	*C*2/c	*C*2/c	*C*2/c
a, Å	35.223(12)	36.60(4)	34.738(5) [−1.4%]	34.714(4) [−5.4%]
b, Å	5.694(11)	5.488(3)	5.7074(5) [+0.2%]	5.7047(5) [+3.9%]
c, Å	9.603(3)	10.054(13)	9.4062(12) [−2.0%]	9.4233(9) [−6.3%]
β, deg	99.248(17)	101.03(6)	98.357(6) [−0.9%]	98.352(5) [−2.7%]
V, Å^3	1901.4(11)	1982(4)	1845.1(4) [−3.0%]	1846.3(3) [−6.8%]
Z	4	4	4	4
ρ_{calc}, g/cm^3	1.336	1.223	1.377	1.376
no. of reflns measured	8431	6084	8453	8221
no. of unique reflns	2189	2096	2109	2125
no. obsd ($I>2\sigma(I)$)	1449	1715	1955	1890
R_1; wR_2	0.062; 0.175	0.064; 0.195	0.045; 0.138	0.040; 0.109
GOF	1.06	1.09	1.10	1.09
temp, °C	−150	−150	−150	−150
d_s, Å	4.80	5.03		
d_{CC}, Å	3.22	3.54		

	EE-EtO	**ZZ-EtO**	poly(**ZZ-EtO**)
crystal system	monoclinic	monoclinic	monoclinic
space group	*C*2/c	*C*2/c	*C*2/c
a, Å	39.539(6)	40.046(19)	38.96(2) [−2.8%]
b, Å	5.7087(10)	5.616(3)	5.714(3) [+1.7%]
c, Å	9.6807(17)	9.632(5)	9.351(5) [−3.2%]
β, deg	90.464(6)	91.05(4)	90.27(2) [−0.9%]
V, Å^3	2185.0(6)	2165.9(18)	2082(2) [−4.0%]
Z	4	4	4
ρ_{calc}, g/cm^3	1.248	1.259	1.310
no. of reflns measured	6588	9161	6651
no. of unique reflns	2390	1257	2323
no obsd ($I>2\sigma(I)$)	1682	873	1063
R_1; wR_2	0.130; 0.381	0.060; 0.151	0.104; 0.299
GOF	1.46	0.99	0.93
temp, °C	−70	−70	−70
d_s, Å	4.84	4.82	
d_{CC}, Å	3.32	3.46	

ZZ-MeO crystals consisted of the lines due to the monomer and the polymer accompanied by a crystal phase separation, despite highly penetrating X-ray radiation conditions. The intensity ratio of lines assigned to the monomer and polymer fractions depended on the conversion, and the positions of the diffraction lines due to the monomer and polymer crystals slightly changed during the reaction. The half-line width values of the **ZZ-MeO** monomer phase increased from 0.12 to 0.39 with the scan number, that is, the conversion. Similar broad diffraction lines were also observed for the polymer crystal phase at the intermediate stage of the reaction, and then the half-line width value decreased to 0.16. The same features of the change in the diffraction lines were observed during the polymerization of **EE-EtO** and **ZZ-EtO**, as shown in Figure 3.

The observed powder X-ray diffraction lines were indexed by comparison with the simulated diffraction profiles using the

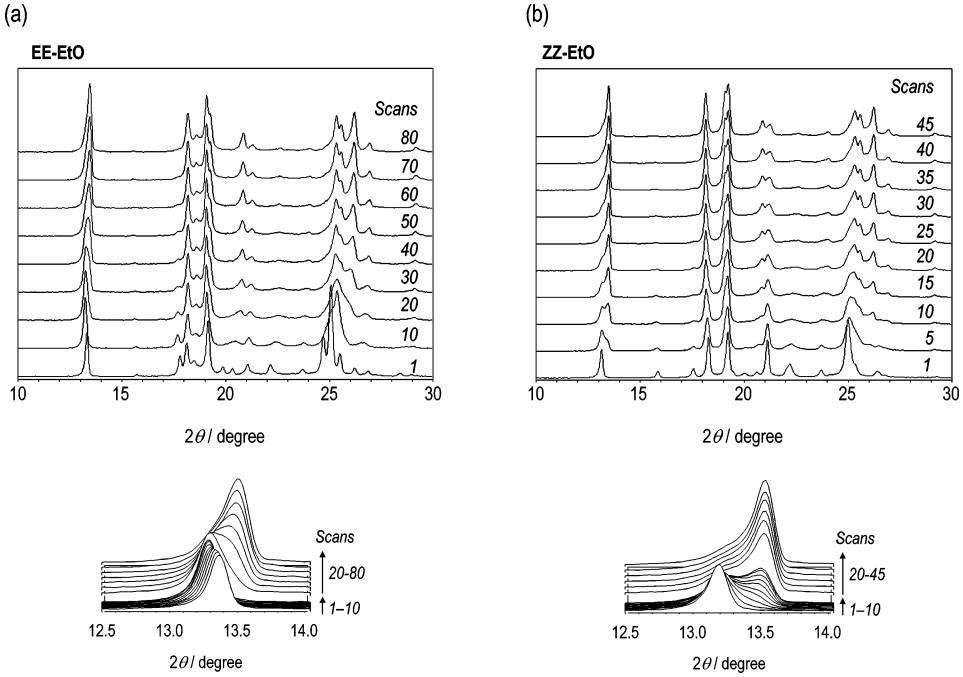

Figure 3. Change in powder X-ray diffraction profiles during the polymerization of (a) **EE-EtO** and (b) **ZZ-EtO** at room temperature. The expanded diffraction lines around 13° were assigned to d_{600}.

Table 2. Change in the Selected Diffraction Line (d_{600}) during Polymerization of EE-MeO and ZZ-MeO

monomer	scan no.	conv. (%)	2θ (deg)	intensity	half-line width
EE-MeO	0	0	15.061	678	0.206
	1	36	15.059	572	0.234
	2	36	14.999	657	0.234
	3	38	14.960	779	0.221
	5	42	14.941	928	0.218
	10	47	14.959	1048	0.235
	20	56	14.999	1170	0.254
	40	65	15.040	1222	0.277
	70	73	15.080	1420	0.282
ZZ-MeO	0	0	14.741	2754	0.120
	1	5	14.759	2512	0.146
	2	9	14.780	1903	0.256
	3	13	14.800/15.119	1837/697	0.325/0.642
	5	15	14.820/15.201	1494/1872	0.389/0.529
	10	16	14.921/15.218	1178/2468	0.388/0.323
	20	22	15.219	8724	0.184
	40	35	15.239	6045	0.166
	70	45	15.238	6463	0.157

data of the corresponding single-crystal structures. Each lattice length was further estimated from the 2θ values of the indexed lines. In the present study, three axes were determined using the d_{600}, d_{310}, and d_{80-2} values, which were observed around 15, 19, and 25° of the 2θ values, respectively. The change in the lattice parameters is shown in Figure 4, as a function of the scan number for the X-ray radiation.

From the diffraction profile of the **EE-MeO** crystals in Figure 2a as well as the plots of the axis length in Figure 4a, the *c*-axis length along the fiber axis of the resulting polymer crystals decreased by ca. 6%. The *a*-axis length once increased to ca. a 1% increment and then decreased, finally leading to shrinking along that axis direction. The *b*-axis length gradually increased. The expanding and shrinking of the lattice length agree well with the results of single-crystal structure analysis of the monomer and polymer, as was already shown in Table 1. Such a continuous change in the crystal lattice was also observed for the polymerization of other muconate monomers, e.g., di(4-chlorobenzyl) (*Z*,*Z*)-muconate and bis(3,4-methylenedioxybenzyl) (*E*,*E*)-muconate.[44]

On the other hand, Figure 2b and Figure 4b indicate that the polymerization of **ZZ-MeO** induces a crystal phase separation from the initial stage of the reaction up to at least about 20% conversion. At a higher conversion, no diffraction line due to the monomer phase was observed. From the plots shown in Figure 4b, it is clear that the polymer phase includes a small change in all the axis lengths, while the monomer phase drastically changes its lattice parameters. This indicates that a large strain is accumulated in the monomer phase rather than in the polymer phase. A change in the half-line width of the diffraction peaks (Table 2) includes the effects of such strain evolved in the mixed crystals of the monomer and polymer, in addition to a decrease in the grain size during the polymerization. Not only the methoxy derivatives but also the ethoxy derivatives provided a similar conclusion. Namely, the polymerization of **EE-EtO** occurred homogeneously, while **ZZ-EtO** occurred heterogeneously with a phase separation, as is clearly shown in the powder X-ray diffraction profiles in Figure 3.

Second, we tried to more precisely determine the structural change in the crystals during the polymerization by *in situ* X-ray

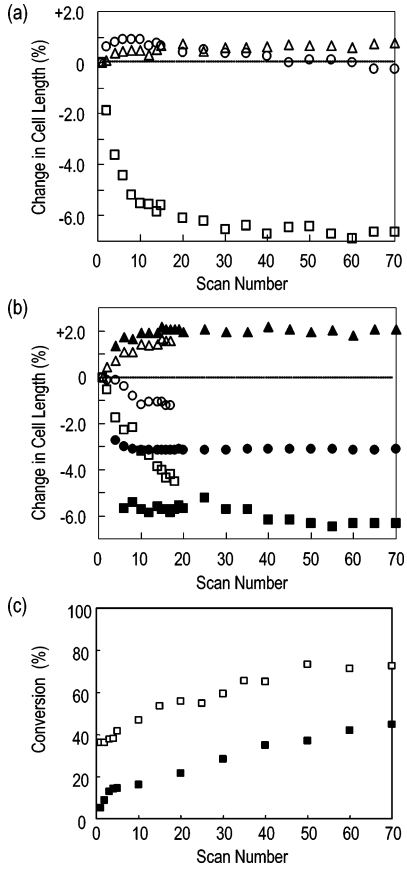

Figure 4. Change in the lattice lengths during the continuous X-ray radiation of (a) **EE-MeO** and (b) **ZZ-MeO**: circle, *a*-axis; triangle, *b*-axis; square, *c*-axis. Opened and filled signs mean the lattice lengths of monomer and polymer phases, respectively, in the plot for **ZZ-MeO**. (c) Relationship between scan number and conversion during the continuous X-ray radiation of (□) **EE-MeO** and (■) **ZZ-MeO**.

single-crystal structure analysis. Repeated X-ray radiation onto the single crystal of **EE-MeO** was carried out at −150 °C and room temperature for the structure determination and the process of polymerization, respectively. The effect of radiation on the polymerization can be ignored at −150 °C. The crystallographic data at each stage of polymerization of the single-crystal structure of **EE-MeO** are summarized in Table 3. No decrease in the reflection numbers and no increase in the R_1 and wR_2 values indicate that the **EE-MeO** crystal retains its single-crystal structure with a high quality even at a high conversion (ca. 50%). The polymer single-crystal structure was determined using the same crystal by the additional 200-kGy γ-radiation after a 10-h X-ray radiation. A disordered structure was observed around the diene moiety of **EE-MeO** during the polymerization irrespective of the conversion, as shown in the ORTEP drawings in Figure 5. The disordered structure was divided into the monomer and polymer structures.

We noticed a maximum value for the lattice parameters of **EE-MeO** (*a*- and *c*-axis lengths, and cell volume) after starting the polymerization within 1-h radiation, i.e., below 30% conversion. The lattice lengths initially include an expansion and consequently the cell volume also temporarily increases at the same time (Figure 6). Such a temporary increase in the lattice constants is due to the coexistence of the monomer and polymer molecules in the common crystal lattice. The coexistence of monomer and polymer structure in a solid solution should cause a strain in the molecular conformation of monomer or polymer as the intermediate structure of the cocrystals. Here, the separated monomer and polymer crystal structures in the cocrystals formed during the polymerization provide us invaluable information about the strain included in the molecules. Therefore, the bond lengths, bond angles, and torsion angles of the monomer and polymer were determined from the separated crystal structures, and the results are summarized in Table 3. The numbering of atoms for the determination is shown in Figure 7.

As a result, no or very little change was observed in the bond lengths and angles for the monomer structure. On the other hand, a drastic change was observed in the polymer conformation. The bond length of C(1P)−C(1′P), C(1P)−C(2P), and C(2P)−C(2′P) already decreased at around 20% conversion. For some bond angles such as C(1P)−C(1′P)−C(2P) and C(1P)−C(2P)−C(2′P) as well as the torsion angle of C(1′P)−C(1P)−C(2P)−C(2′P), extraordinary angle values are observed. Seemingly, the structural strain tends to be accumulated in the polymer structure.

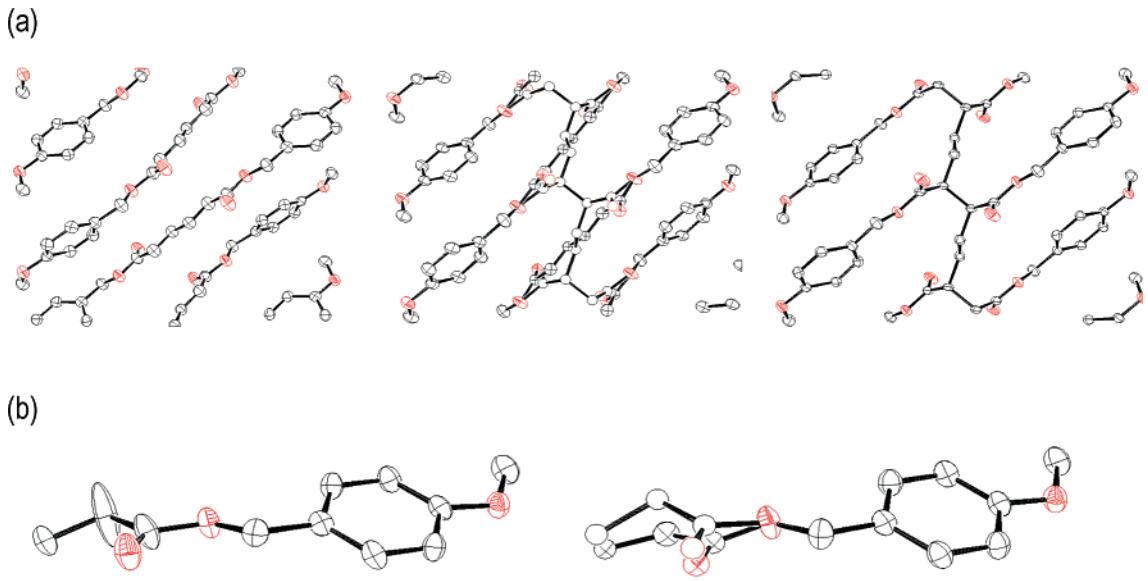

Figure 5. (a) Change in ORTEP drawings during the polymerization of **EE-MeO**. Initial monomer structure (left), intermediate structure with a site occupancy factor of 52.6% for poly(**EE-MeO**) (center), and polymer structure obtained by γ-radiation polymerization (right). Hydrogen atoms are omitted for clarity. Thermal ellipsoids are plotted at the 50% probability level. (b) Expanded disordered structures before and after separation into the monomer and polymer structures.

Table 3. Change in the Single-crystal Structure of EE-MeO during the Polymerization

radiation time, h	0	0.17	0.33	0.5	1	4	10	polymer
(conv, %)[a]	(0)	(19.8)	(20.9)	(25.2)	(36.3)	(40.0)	(52.6)	(100)
a, Å	35.223(12)	35.40(3)	35.66(3)	35.330(15)	35.254(14)	35.289(12)	35.066(16)	34.68(10)
b, Å	5.694(11)	5.677(4)	5.712(3)	5.687(2)	5.714(2)	5.6995(19)	5.687(2)	5.714(10)
c, Å	9.603(3)	9.614(8)	9.662(7)	9.574(3)	9.551(3)	9.516(4)	9.466(3)	9.43(2)
β, deg	99.248(17)	99.59(4)	99.00(3)	99.224(19)	98.736(15)	98.96(3)	98.89(3)	98.21(8)
V, Å^3	1901.4(11)	1905(3)	1944(2)	1898.7(13)	1901.7(12)	1890.5(12)	1865(13)	1851(7)
ρ_{calc}, g/cm^3	1.336	1.333	1.307	1.338	1.336	1.343	1.362	1.372
no. of reflns measured	8431	8425	7987	8268	8156	7155	7160	2125
no. of unique reflns	2189	2199	2201	2183	2187	2174	2083	2125
no. obsd ($I > 2\sigma(I)$)	1449	1451	1390	1405	1347	1348	1306	1336
R_1	0.062	0.055	0.053	0.058	0.054	0.063	0.062	0.057
wR_2	0.175	0.148	0.128	0.152	0.149	0.173	0.164	0.152
GOF	1.06	1.03	0.99	1.07	1.08	1.09	1.07	1.02
C(1 M)−C(1′M), Å	1.409(5)	1.349(15)	1.457(9)	1.452(10)	1.446(12)	1.430(14)	1.422(17)	
C(1 M)−C(2 M), Å	1.342(3)	1.353(9)	1.348(5)	1.338(6)	1.340(7)	1.336(7)	1.330(10)	
C(2 M)−C(3M), Å	1.462(3)	1.466(5)	1.481(5)	1.471(6)	1.480(6)	1.465(8)	1.491(10)	
C(1P)−C(1′P), Å		1.51(4)	1.24(4)	1.24(4)	1.35(2)	1.33(2)	1.352(17)	1.322(5)
C(1P)−C(2P), Å		1.60(3)	1.53(2)	1.53(2)	1.498(13)	1.513(12)	1.500(10)	1.509(4)
C(2P)−C(2′P), Å		1.63(7)	1.57(5)	1.57(5)	1.56(3)	1.58(2)	1.58(2)	1.588(5)
C(2P)−C(3P), Å		1.47(3)	1.56(2)	1.500(19)	1.521(12)	1.514(12)	1.479(9)	1.51(44)
C(1 M)−C(1′M)−C(2 M), deg	123.3(3)	125.0(10)	122.6(5)	122.1(6)	123.0(7)	124.1(7)	122.7(10)	
C(1 M)−C(2 M)−C(3M), deg	121.7(2)	123.5(4)	121.6(3)	121.2(4)	121.8(4)	122.3(5)	121.3(7)	
C(2 M)−C(3M)−O(1 M), deg	125.3(2)	122.5(5)	122.1(5)	124.2(4)	122.0(5)	122.2(6)	120.9(7)	
C(1P)−C(1′P)−C(2P), deg		109.3(18)	130(3)	127(2)	125.2(15)	123.0(13)	124.1(11)	123.8(3)
C(1P)−C(2P)−C(3P), deg		96.8(19)	110.5(12)	110.9(12)	110.3(8)	110.2(7)	110.6(6)	110.24(19)
C(1P)−C(2P)−C(2′P), deg		124.4(18)	114.2(12)	112.9(11)	113.6(8)	112.2(7)	111.8(5)	112.7(3)
C(2P)−C(3P)−O(1P), deg		138(3)	135.2(19)	126.2(15)	127.8(10)	127.1(9)	127.1(8)	125.1(2)
C(1′P)−C(1P)−C(2P)−C(2′P), deg		72(2)	111(3)	113(2)	111.4(13)	111.7(12)	108.9(10)	103.9(3)

[a] Determined on the basis of site occupancy factors of monomer and polymer structures.

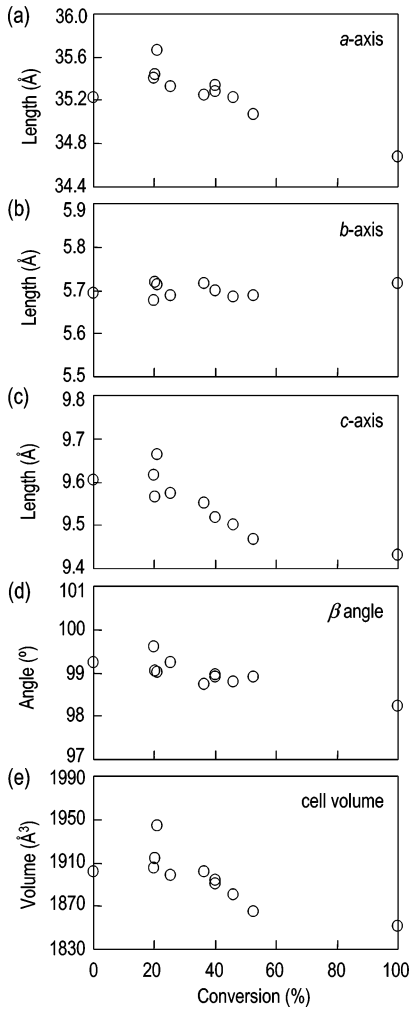

Figure 6. Changes in (a) *a*-axis length, (b) *b*-axis length, (c) *c*-axis length, (d) β-angle, and (e) cell volume of **EE-MeO** during the polymerization.

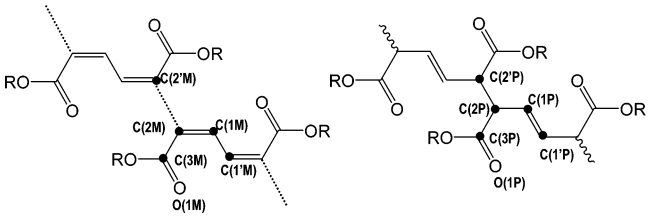

Figure 7. Numbering of atoms for determination of bond lengths, bond angles, and torsion angles for the monomer (left) and polymer (right) structures.

The bond angles and the torsion angles may play an important role in accepting a mismatch between the monomer and polymer structures and in avoiding the collapse of single crystals. The initial change in the lattice parameters, already mentioned above, is ascribed to the produced polymer chain in the monomer crystal. The structural strain is tend to be concentrated in the polymer structure rather than in the monomer structure.

We now discuss a reaction model for the solid-state polymerization based on the results obtained in the present study. Topochemical polymerization includes two kinds of polymerization mechanisms as the extreme cases,[16,17] as shown in Figure 8. One is the homogeneous reaction mechanism, as was seen in the polymerization of **EE-MeO**. In this model, polymerization occurs at the random positions of the crystals, and both the monomer and polymer molecules include structural strain during the reaction. This forms a solid solution and no phase separation is observed at the intermediate stage of the reaction. Therefore, we can directly observe a change in the single-crystal structure from 0 to 100% conversion throughout the reaction. Another is the heterogeneous reaction mechanism, being observed for **ZZ-MeO**. The reaction starts preferentially near specific defect sites and accompanies the nucleation of a polymer phase. The produced polymer forms a new domain in the monomer crystals in the process of the polymerization, and consequently, phase separation is observed at the intermediate stage. In the latter model, the strain is possibly concentrated around the interface of the monomer and polymer phases, and the polymerization is

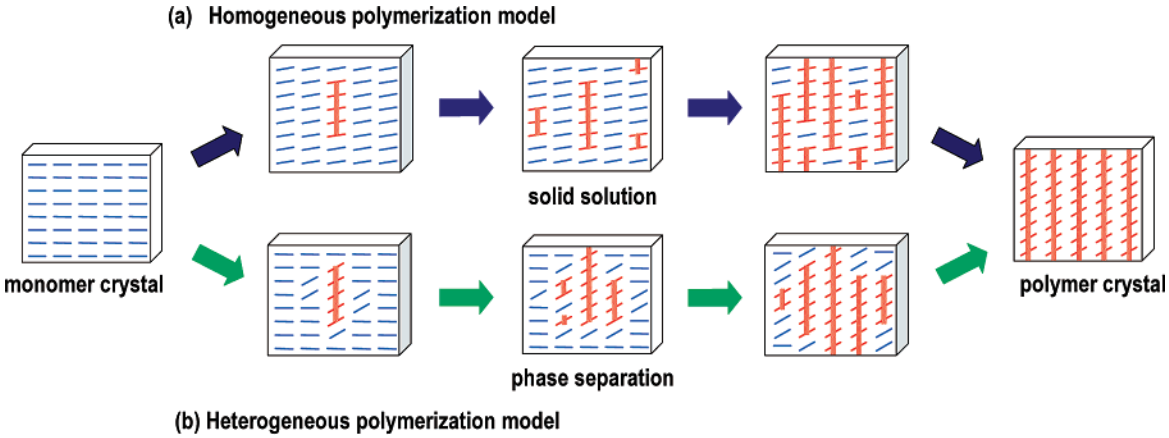

Figure 8. Schematic model for (a) homogeneous polymerization mechanism and (b) heterogeneous polymerization mechanism.

accelerated near the phase boundary. This mechanism eventually leads to the destruction of the mother crystal. However, polymer single crystals can be obtained as the final product after complete reactions. This is actually evidenced by the successful crystal structure analysis with a high accuracy for the polymer single crystals of **ZZ-MeO** obtained by γ-ray radiation polymerization. The rearrangement of the molecules at the grain boundary may occur during the polymerization, leading to the formation of polymer single crystals, although the intermediate stage includes a phase separation. These models were similar to those previously reported,[17] but in our model, a conformational change in the unreacted monomer domains is emphasized for the homogeneous polymerization model. Such a change often results in the drastic phase transition of the whole crystals from the starting structure into the structure of the product. The model proposed in the present study is specific to the polymerization that undergoes via a chain reaction mechanism in the solid state. This model includes the strain accumulated in the whole crystals during the reaction because of the presence of long-chain polymer molecules as the products. For the reactions of low-molecular-weight compounds yielding the corresponding low-molecular-weight products such as the isomer or dimer products, the reactivity in the solid state has exclusively been explained by the mobility of the atom in the solid state. A free volume surrounding a reacting center also important because the intermolecular space can act as a buffer to reduce the strain evolved during the reactions.[62−66]

Actual polymerization proceeds in the mechanism of the homogeneous or heterogeneous reaction, depending on a change in the crystal lattices, and the movement of atoms, and the crystal size and quality. The values of monomer stacking distance (d_s) and the carbon-to-carbon distance between the reacting monomers (d_{CC})[39] are smaller for the **EE-MeO** (d_s = 4.80 Å, d_{CC} = 3.22 Å) than those for **ZZ-MeO** (d_s = 5.03 Å, d_{CC} = 3.54 Å), as shown in Table 1. A difference in these distance values agrees well with the conclusion that the polymerizations of **EE-MeO** and **ZZ-MeO** occur via a homogeneous and heterogeneous reaction mechanism, respectively. In the case of the ethoxy derivatives, the d_s values are the same; d_s = 4.84 and 4.82 Å for **EE-EtO** and **ZZ-EtO**, respectively. The d_{CC} value of **EE-EtO** (d_{CC} = 3.32 Å) is smaller than that of **ZZ-EtO** (d_{CC} = 3.46 Å). The homogeneous polymerization mechanism requires the least movement of atoms during the reaction, and therefore, the smaller d_{CC} value is favored to achieve homogeneous polymerization to produce solid solutions during the reaction of **EE-EtO**.

Conclusions

We have reported the structural changes in the muconic ester crystals in the process of polymerization via a crystal-to-crystal transformation. The crystal structures of **EE-MeO** and **ZZ-MeO,** which give polymers with the same structure, were determined by single crystal analysis. The obtained crystallographic data clearly showed that a change in lattice parameters during the polymerization of **ZZ-MeO** is greater than those for **EE-MeO**. A structural change during the polymerization was also monitored by continuous powder X-ray diffraction, and we have discussed a reaction mechanism for the solid-state polymerization via a chain reaction mechanism, homogeneous and heterogeneous reaction mechanisms. In the homogeneous reaction mechanism, polymers are produced at a random position in the crystals, and the monomer and polymer molecules form a solid solution. A strain is included in both of the monomer and polymer. In contrast, the reaction occurs preferentially at specific defect sites, and consequently, a phase separation occurs during the polymerization via a heterogeneous reaction mechanism. Moreover, *in situ* single-crystal X-ray analysis of the polymerization of **EE-MeO** via a homogeneous reaction mechanism revealed that the lattice lengths show expansion at the initial stage of the reaction, even for the fiber axis, which is followed by large shrinking. Such a temporary increase causes a strained intermediate structure due to a mismatch between the monomer and polymer structures. In our previous paper, we discussed the shrinking and expanding polymerizations depending on the monomer stacking structure in a columnar assembly in the crystals.[44] In the present study, furthermore, the homogeneous and heterogeneous polymerization mechanism has been discussed. The role of the structural strain in the crystals is important to clarify the relation to the polymerization mechanism. Very recently, we found experimental evidence for an induction period and acceleration of the polymerization related to the crystal strain. We are now investigating to fully understand the mechanism of the solid-state polymerization of 1,3-diene and the other unsaturated monomers.

Acknowledgment. This work was supported by Grants-in-Aid for Scientific Research on Priority Areas (Area No. 432, No. 16072215) and for Scientific Research (No. 16350067) from the Ministry of Education, Culture, Sports, Science, and Technology (MEXT) of Japan. We gratefully thank Prof. Kunio Oka, Osaka Prefecture University, for his kind assistance with the γ-radiation experiment.

Supporting Information Available: X-ray crystallographic information files (CIF) for **EE-MeO** and **ZZ-MeO**. This material is available free of charge via the Internet at http://pubs.acs.org.

References and Notes

(1) MacNicol, D. D., Toda, F., Bishop, R., Eds. *Comprehensive Supramolecular Chemistry, Vol. 6, Solid State Supramolecular Chemistry: Crystal Engineering*; Pergamon: Oxford, U.K., 1996.
(2) Matsumoto, A. In *Handbook of Radical Polymerization*; Matyjaszewski, K., Davis, T. P., Eds.; Wiley: New York, 2002; Chapter 13, p 691.
(3) Toda, F., Ed. *Topics in Current Chemistry 254, Organic Solid State Reactions*; Springer: Berlin, 2005.
(4) Kaupp, G. *Top. Curr. Chem.* **2005**, *254*, 95.
(5) Braga, D.; Grepioni, F. Eds. *Making Crystals by Design: Methods, Techniques and Applications*; Wiley-VCH: Weinheim, Germany, 2007.
(6) Cheng, K.; Foxman, B. M. *J. Am. Chem. Soc.* **1977**, *99*, 8102.
(7) Nakanishi, H.; Jones, W.; Thomas, J. M.; Hursthouse, M. B.; Motevalli, M. *J. Phys. Chem.* **1981**, *85*, 3636.
(8) Enkelmann, V.; Wegner, G.; Novak, K.; Wagener, K. B. *J. Am. Chem. Soc.* **1993**, *115*, 10390.
(9) Takahashi, S.; Miura, H.; Kasai, H.; Okada, S.; Oikawa, H.; Nakanishi, H. *J. Am. Chem. Soc.* **2002**, *124*, 10944.
(10) Gao, X.; Friščić, T.; MacGillivray, L. R. *Angew. Chem., Int. Ed.* **2004**, *43*, 232.
(11) Turowska-Tyrk, I.; Bakowicz, J.; Scheffer, J. R.; Xia, W. *CrystEngCommun* **2006**, *8*, 616.
(12) Cohen, M. D.; Schmidt, G. M. J. *J. Chem. Soc.* **1964**, 1996.
(13) Schmidt, G. M. J. *Pure Appl. Chem.* **1971**, *27*, 647.
(14) MacGillivray, L. R. *CrysEngCommun* **2002**, *4*, 37.
(15) Braga, D. *Chem. Commun.* **2003**, 2751.
(16) Wegner, G. *Pure Appl. Chem.* **1977**, *49*, 443.
(17) Enkelmann, V. *Adv. Polym. Sci.* **1984**, *63*, 91.
(18) Tieke, B. *Adv. Polym. Sci.* **1985**, *71*, 79.
(19) Hasegawa, M. *Adv. Phys. Org. Chem.* **1995**, *30*, 117.
(20) Njus, J. M.; Sandman, D. J.; Yang, L.; Foxman, B. M. *Macromolecules* **2005**, *38*, 7645.
(21) Sun, A. W.; Lauher, J. W; Goroff, N. S. *Science* **2006**, *312*, 1030.
(22) Itoh, T.; Nomura, S.; Uno, T.; Kubo, M.; Sada, K.; Miyata, M. *Angew. Chem., Int. Ed.* **2002**, *41*, 4306.
(23) Matsumoto, A.; Matsumura, T.; Aoki, S. *J. Chem. Soc., Chem. Commun.* **1994**, 1389.
(24) Matsumoto, A.; Odani, T. *Macromol. Rapid Commun.* **2001**, *22*, 1195.
(25) Matsumoto, A. *Polym. J* **2003**, *35*, 93.
(26) Matsumoto, A. *Top. Curr. Chem.* **2005**, *254*, 263.
(27) Linhart, W.; Peters, F.; Lehmann, W.; Schwarz, K.; Schilling, A. F.; Amling, M.; Rueger, J. M.; Epple, M. *J. Biomed. Mater. Res.* **2001**, *54*, 162.
(28) Sasaki, T.; Hayashibara, K.; Suzuki, M. *Macromolecules* **2003**, *36*, 279.
(29) Kimura, K.; Kohama, S.; Yamashita, Y. *Macromolecules* **2002**, *35*, 7545.
(30) Meng, H.; Perepichka, D. F.; Wudl, F. *Angew. Chem., Int. Ed.* **2003**, *42*, 658.
(31) Nery, J. G.; Bolbach, G.; Weissbuch, I.; Lahav, M. *Angew. Chem., Int. Ed.* **2003**, *42*, 2157.
(32) Matsumoto, A.; Matsumura, T.; Aoki, S. *Macromolecules* **1996**, *9*, 423.
(33) Matsumoto, A.; Yokoi, K.; Aoki, S.; Tashiro, K.; Kamae, T.; Kobayashi, M. *Macromolecules* **1998**, *31*, 2129.
(34) Tashiro, K.; Kamae, T.; Kobayashi, M.; Matsumoto, A.; Yokoi, K.; Aoki, S. *Macromolecules* **1999**, *32*, 2449.
(35) Tashiro, K.; Zadorin, A. N.; Saragai, S.; Kamae, T.; Matsumoto, A.; Yokoi, K.; Aoki, S. *Macromolecules* **1999**, *32*, 7946.
(36) Matsumoto, A.; Odani, T.; Chikada, M.; Sada, K.; Miyata, M. *J. Am. Chem. Soc.* **1999**, *121*, 11122.
(37) Matsumoto, A.; Nagahama, S.; Odani, T. *J. Am. Chem. Soc.* **2000**, *122*, 9109.
(38) Matsumoto, A.; Katayama, K.; Odani, T.; Oka, K.; Tashiro, K.; Saragai, S.; Nakamoto, S. *Macromolecules* **2000**, *33*, 7786.
(39) Matsumoto, A.; Tanaka, T.; Tsubouchi, T.; Tashiro, K.; Saragai, S.; Nakamoto, S. *J. Am. Chem. Soc.* **2002**, *124*, 8891.
(40) Matsumoto, A.; Sada, K.; Tashiro, K.; Miyata, M.; Tsubouchi, T.; Tanaka, T.; Odani, T.; Nagahama, S.; Tanaka, T.; Inoue, K.; Saragai, S.; Nakamoto, S. *Angew. Chem., Int. Ed.* **2002**, *41*, 2502.
(41) Tanaka, T.; Matsumoto, A. *J. Am. Chem. Soc.* **2002**, *124*, 9697.
(42) Matsumoto, A.; Furukawa, D.; Nakazawa, H. *J. Polym. Sci., Part A, Polym. Chem.* **2006**, *44*, 4952.
(43) Nagahama, S.; Tanaka, T.; Matsumoto, A. *Angew. Chem., Int. Ed.* **2004**, *43*, 3811.
(44) Matsumoto, A.; Furukawa, D.; Mori, Y.; Tanaka, T.; Oka, K. *Cryst. Growth Des.* **2007**, *7*, 1078.
(45) Chemla, D. S., Zyss, J., Eds. *Nonlinear Optical Properties of Organic Molecules and Crystals*; Academic Press: New York, 1987.
(46) Zuilhof, H.; Barentsen, H. M.; van Dijk, M.; Sudhölter, E. J. R.; Hoofman, R. J. O. M.; Siebbeles, L. D. A.; de Haas, M. P.; Warman, J. M. *Supramolecular Photosensitive and Electroactive Materials*; Nalwa, H. S., Ed.; Academic Press: New York, 2001; p 339.
(47) Wegner, G. *Makromol. Chem.* **1971**, *145*, 85.
(48) Kaiser, J.; Wegner, G.; Fischer, E. W. *Isr. J. Chem.* **1972**, *10*, 157.
(49) Enkelmann, V.; Leyrer, R. J.; Schleier, G.; Wegner, G. *J. Mater. Sci.* **1980**, *15*, 168.
(50) Hasegawa, M. *Chem. Rev.* **1983**, *83*, 507.
(51) Tieke, B. *J. Polym. Sci., Polym. Chem. Ed.* **1984**, *22*, 391.
(52) Tieke, B.; Chapuis, G. *J. Polym. Sci., Polym. Chem. Ed.* **1984**, *22*, 2895.
(53) Baughman, R. H. *J. Appl. Phys.* **1972**, *43*, 4362.
(54) Baughman, R. H.; Yee, K. C. *J. Polym. Sci., Macromol. Rev.* **1978**, *13*, 219.
(55) Chance, R. R.; Patel, G. N. *J. Polym. Sci., Polym. Phys. Ed.* **1978**, *16*, 859.
(56) Bloor, D.; Koski, L.; Stevens, G. C.; Preston, F. H.; Ando, D. J. *J. Mater. Chem.* **1975**, *10*, 1678.
(57) Enkelmann, V.; Leyrer, R. J.; Wegner, G. *Makromol. Chem.* **1987**, *180*, 1787.
(58) Kollmar, C.; Sixl, H. *J. Chem. Phys.* **1987**, *87*, 5541.
(59) Bassler, H. *Adv. Polym. Sci.* **1984**, *63*, 1.
(60) Sixl, H. *Adv. Polym. Sci.* **1984**, *63*, 49.
(61) Matsumoto, A.; Tanaka, T.; Oka, K. *Synthesis* **2005**, 1479.
(62) Cohen, M. D. *Angew. Chem., Int. Ed. Engl.* **1975**, *14*, 386.
(63) Ohashi, Y.; Yanagi, K.; Kurihara, T.; Sasada, Y.; Ohgo, Y. *J. Am. Chem. Soc.* **1981**, *103*, 5805.
(64) Gavezzotti, A. *J. Am. Chem. Soc.* **1983**, *105*, 5220.
(65) Kaupp, G. *CrystEngCommun* **2003**, *5*, 117.
(66) Moorthy, J. N.; Venkatakrishnan, P.; Savitha, G.; Weiss, R. G. *Photochem. Photobio. Sci.* **2006**, *5*, 903.

MA070802F